Application of zirconia thermal barrier coating on the surface of pulling-straightening roller

Feng Zhang[1], Dengyue Sun[1*], Jiuming Xie[2], Shimin Xu[1], Huagui Huang[1], Jun Li[1], Haitao Hou[1], Jin Wu[2]

[1] National Engineering Research Center for Equipment and Technology of Cold Strip Rolling, Yanshan University, Qinhuangdao 066004, China
[2] School of Mechanical Engineering, Tianjin Sino-German University of Applied Sciences, Tianjin 300350, China

Email: sdy@ysu.edu.cn

ABSTRACT

This paper aims to extend the service life of pulling-straightening rollers. For this purpose, a zirconia thermal barrier coating (TBCs) was prepared on the roller surface, and the properties of TBCs prepared by plasma spraying and laser remelting were investigated separately. Then, the surface temperature distribution of roller was calculated with ABAQUS. Next, the conventional zirconia and nanoscale zirconia were coated on H13 steel, and observed using a confocal laser scanning microscope and a thermomechanical simulator. It is found that TBCs can reduce the roll surface temperature and thus the thermal stress; both laser remelting and nanoscale zirconia can improve the quality and thermal shock resistance of the coating. This research on TBC properties lays a solid basis for the application of the TBC on pulling-straightening roller.

Keywords: Laser Remelting, Nano Zirconia, Thermal Barrier Coating (TBC), Pulling-Straightening Roller.

1. INTRODUCTION

The surface quality of continuous casting billet, a key determinant of metal yield and construction cost, directly hinges on that of the pulling-straightening roller. Working under extreme environments, the roller may subject to surface problems like cracking and exfoliation. To prevent such damages, it is necessary to lower the surface temperature and improve the working environment of the roller [1].

One of the most popular technologies for high-temperature component protection is thermal barrier coating (TBC) [2]. The TBC has been extensively used in fields like aviation, gas power generation and chemical engineering, aiming to extend the service life of hot end components. Plasma spraying is the most mature TBC preparation method. On the upside, plasma-sprayed TBC is featured by cost-effectiveness, fast deposition, and wide applicability; on the downside, such a TBC has a high porosity and many defects in its layered structure. The porous and defected structure may lower the bonding strength, induce surface flaking, and shorten the service life of the coating [3].

The plasma-sprayed TBC can be further enhanced by laser remelting, an emerging surface engineering technology. Laser remelting helps to improve the microstructure, eliminate the lamellar structure, decrease the porosity and improve the density of plasma-sprayed coating. Moreover, the technology promotes the homogeneous diffusion of elements at the interface, and the metallurgical bonding between coating and substrate interface, thereby enhancing the bonding strength of coating and matrix [4].

Much research has been done on the laser remelting technology. Munez et al. verified that laser remelting can improve the quality of thermal spraying coating by reducing the coating porosity [5]. Liu et al. revealed that, through laster remelting, the bonding of coating-substrate interface shifted from mechanical bonding to metallurgical bonding, and the coating had a stronger corrosion resistance [6]. Probing into the damage mechanism of TBCs after laser remelting, Fan et al. concluded that the coating damages are related to the surface morphology and segmented cracks [7].

To improve the thermal shock resistance of pulling-straightening roller, zirconia coating is a viable option with its low thermal conductivity, strong oxidation resistance and good high-temperature stability [8-9]. During the plasma spraying and laser remelting, the ZrO_2 is very likely to shift among its three phases: tetragonal, cubic and monoclinic phases. Hence, the Y_2O_3 should be added by the mass fraction of 8% to prevent the phase change and maintain the stability of the coating composition [10-11].

In this work, the TBC system consists of two layers: an oxidation-resistant metallic bond coat, and a porous thermal-insulting ceramic topcoat. The former is made of NiCrAlY

alloy, while the latter 8 wt% Y2O3 -stabilized zirconia (8YSZ). The TBCs were firstly prepared by plasma spraying and then treated by laser remelting to evaluate their microstructure and thermal shock behaviours. In addition, the author analysed the effect of the coating on the surface temperature field of the roller by ABAQUS, and compared the performance of zirconia coatings with different specifications.

2. EFFECT OF TBCS ON ROLLER SURFACE TEMPERATURE

### 2.1. Finite-element simulation (FEM)

This section probes into the effect of TBCs on the surface temperature of pulling-straightening roller. For computing efficiency, the 2D model was employed without sacrificing the calculation accuracy [12]. The geometric model and the mesh division are shown in Figure 1(a). The roller was treated as a deformable body and divided into 4-node quadrilateral temperature/displacement elements. Specifically, the outer grid cells of the roller and the top grid cells of the metal slab are 2mm in size. The coating and the top surface of the roller share the same grid but differ in mesh type. Hence, the outer ring of the coated roller appears as a bright layer (Figure 1(b)). The ceramic layer was made of zirconia, whose thermal physical parameters are presented in Table 1 [13]. The thermal physical properties of the matrix material H13 are listed in Table 2.

**Table 1.** Thermal physical properties of zirconia

Temperature (K)	298	600	900	1200	1500
Density (kg/m3)	6037	--	--	--	--
Thermal conductivity (W/(m.K))	1.576	1.697	1.815	1.937	2.046
Specific heat capacity (J/(kg.K))	455.58	571.02	607.02	631.57	605.48

Table 2. Thermal physical properties of H13

Temperature (K)	298	600	900	1200
Elastic modulus(GPa)	210	--	165	--
Coefficient of expansion (10-6/K)	9.1	10.3	11.5	12.2
Thermal conductivity (W/(m.K))	32.23	--	21.41	--
Specific heat capacity (J/(kg.K))	461	481	514	520
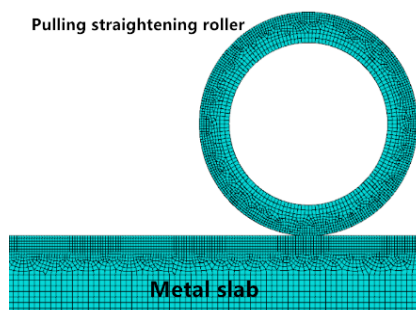
(a) Geometric model
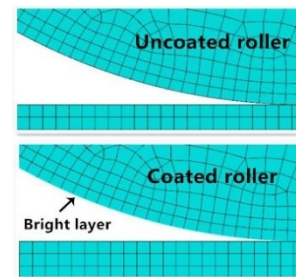
(b) Local amplification

Figure 1. Geometric model

2.2. Initial and boundary conditions

In the ABAQUS-based FEM, the accuracy of the boundary conditions relies heavily on that of the simulated results. In actual practice, the pulling-straightening roller is contacted with the high-temperature slab, such that the heat of the slab flows into the roller uninterruptedly across the contact zone. This is the main source of heat flowing into the roller. However, the roller temperature will decrease rapidly under cross-ventilation and water cooling [14], So it is necessary to consider the influence of convective cooling in the boundary condition [15]. With the rotation of the roller, the temperature near the slab increases. After the roller disengages itself from the slab, its temperature gradually declines. In this way, the roller surface temperature exhibits a periodic variation trend.

For the sake of accuracy, the heat transfer between the roller, the slab, the air and the cooling water was taken into account in the simulation. Table 3 shows the heat transfer coefficients used in the simulation [16]. At the beginning of simulation, all roller nodes were at the room temperature (25℃), and the casting billets were all 1,000℃. Both the roller and the slab were set as deformable bodies, and the rotation speed of the roller was set to 0.01m/s.

Table 3. Heat exchange coefficients

Unit: (W/(m2·℃))	Roller and slab	Roller and cooling water	Roller and air
Uncoated roller	6426.2	1511.4	16.5
Coated roller	2500	1511.4	11.7

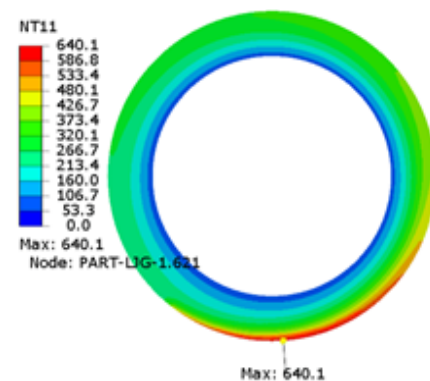### 2.3. Analysis of simulation results

Figure 2. Temperature distribution of uncoated roller

After several calculations, the temperature stabilised after the roller completed 6 rotations. Then, the temperature field distribution pattern and temperature trend were discussed

based on the node temperature and temperature graph. According to temperature distribution of uncoated roller in Figure 2, the surface temperature dropped by 390°C from the peak value of 640°C to the valley value of 250°C. According to the temperature distribution of coated roller in Figure 3, the surface temperature dropped by 265°C from the peak value of 445°C to the valley value of 180°C. It is clear that the coated roller lagged behind the uncoated one in the peak surface temperature and the temperature drop. The peak temperature of roller surface was synthetized and recorded in Figure 4.
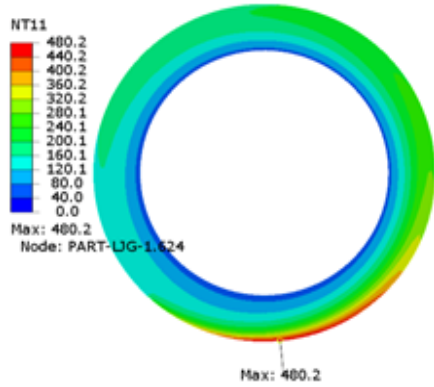

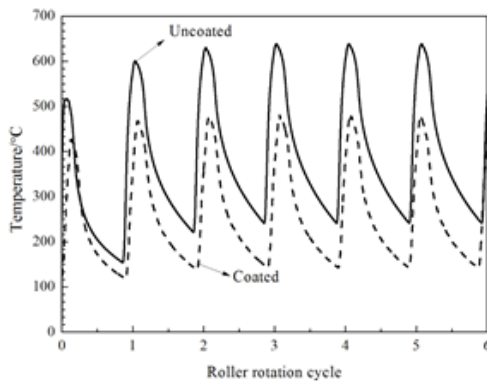**Figure 3.** Temperature distribution of coated roller

Figure 4. Peak temperature of roller surface

The FEM results show that: in the uncoated scenario, the roller surface temperature rose rapidly in the deformed area, and then declined fast under air convection and water cooling. The heat shock is very obvious. The dramatic temperature change on roller surface resulted in a great heat stress, a catalyst of thermal fatigue cracking. Under the joint action of heat stress and other factors, the cracks continued to propagate and eventually developed into macro cracks, leading to surface exfoliation. With the application of 8YSZ TBCs, the roller surface temperature and heat stress dropped noticeably. The decline curbed the thermal cracking and increased the service life of the roller.

3. MEASUREMENT OF ROLLER SURFACE TEMPERATURE

The temperature measurement was carried out on a two-high rolling mill (Figure 5). The effect of TBCs on roller surface temperature was tested to verify the correctness of the FEM results. The roll surface coating of the 100mm-long test roller was plasma sprayed using a plasma spraying unit (Sulzer Metco). The cylindrical surface diameter of the roller was 90mm. The roller surface temperature was measured by a LaserSight infrared thermometer (Optris). A cast copper heating plate was employed to heat up the roller surface to 500°C. The HS-G type bidirectional inner tube fixed rotary joint was adopted to pour the cooling water into the roller and water cool the inner wall of the test roller.

Figure 5. Two-high rolling mill

3.1 FEM of the test roller

The FEM of the test roller was performed on ABAQUS according to the test conditions. The boundary conditions and mesh generation method were the same with the previous FEM, other than the heating method. The FEM results are illustrated in Figure 6.
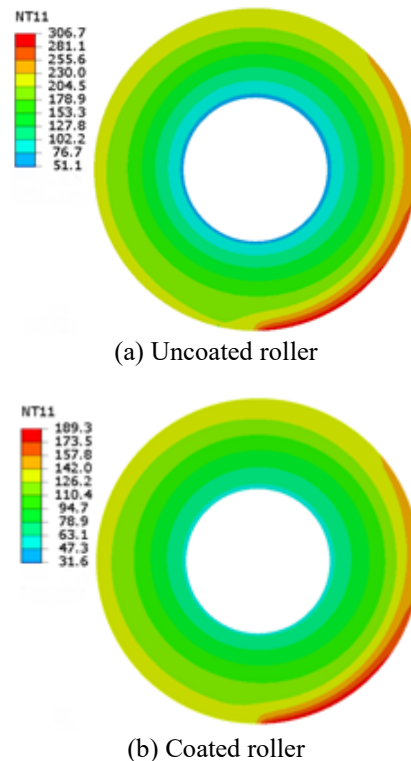

(a) Uncoated roller

(b) Coated roller

Figure 6. FEM under the test conditions

As shown to Figure 6, under the test conditions, the surface temperature of the uncoated roller was maximized at about 306°C, and minimized at about 204°C. After the roller surface was coated with 8YSZ, the maximum surface temperature dropped by 117°C to about 189°C, and the minimum surface

temperature dropped by 78°C to about 126°C.

3.2 Measurement of roller surface temperature

Five temperature measuring points were selected at an interval of 20mm along the length direction of the roller surface. The outmost measuring point was 10mm away from the end face of the roller. The location of the measuring points is shown in Figure 7.
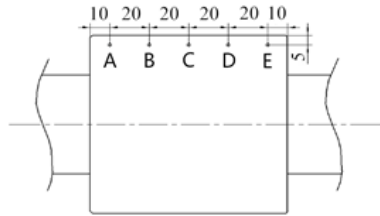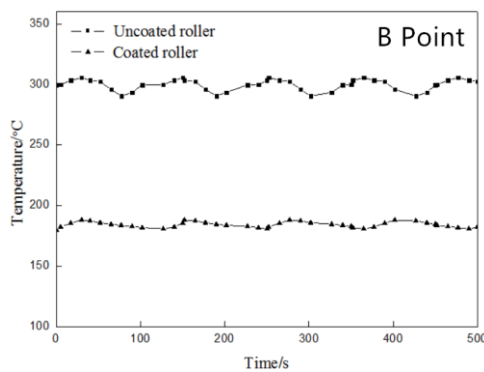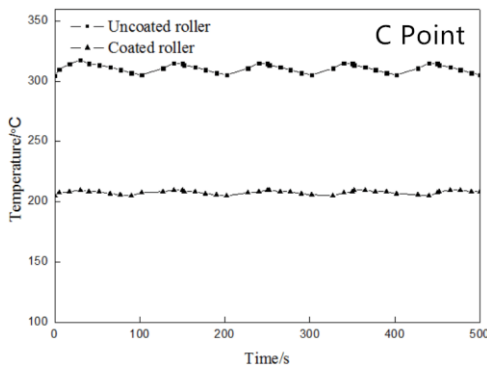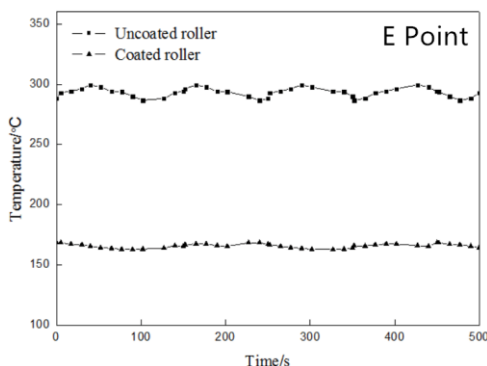

Figure 7. Location of measuring points

(a) Point B temperature

(b) Point C temperature

(c) Point E temperature

Figure 8. Steady-state temperature curves of three test points

On the roller surface, there was a symmetrical relationship between points A and E, and between points B and D. Hence, each pair of points shared a basically consistent trend of temperature. In view of the symmetry, points B, C and E were taken to measure the steady-state temperature variation curves of coated and uncoated test rollers. The measured temperature is shown in Figures 8 (a), (b) and (c).

From Figure 8, it can be seen that the average temperature of points B, C and E on the uncoated roller surface was about 300°C and that on the coated roller surface was about 180°C. The measured temperatures on the roller surface coincide with those obtained by ABAQUS simulation, which verifies the reliability of the ABAQUS simulation in determining the surface temperature distribution of pulling-straightening roller.

4. MICROSCOPIC ANALYSIS OF LASER REMELTING EFFECT ON COATING PROPERTIES

4.1 Preparation of coatings

TBCs, consisting of a 100μm-thick bond coat and a 200μm-thick ceramic topcoat, were deposited on a hot-work die steel (H13) substrate by plasma spraying and laser remelting. The spraying parameters are presented in Table 4. The preparation was implemented through the following steps. First, a bond coat of Ni–19Cr–5Al–1.5Y (wt%) was deposited onto the substrate; then, 8YSZ powders were plasma-sprayed onto the surface of the bond coat; finally, a part of the plasma-sprayed coating was remelted by a 2kW CO_2 laser (velocity: 2mm/s; spot size: Φ1.5mm; overlap rate: 30%).

Table 4. Plasma spraying parameters

| Spraying Parameters	NiCrAlY Layer	ZrO_2-8%Y_2O_3 Layer
Spraying voltage (V)	60	58.3
Spraying current (A)	550	500
Master gas flow (L/min)	41	50
Auxiliary gas flow (L/min)	4.9	8
Spraying distance (mm)	100	120
Feeding rate (g/min)	26	15
Spraying speed (mm/s)	70	70

4.2 Microstructure analysis of TBCs

The surface and the fractured cross-section morphology of the coatings were observed with an S-4800 field emission SEM (Hitachi).

According to the surface morphology of plasma-sprayed coating in Figure 9 (a), the YSZ coating exhibited a typical structure of plasma-sprayed ceramic powders, and visible particles not fully melted on the coating surface. The heavy presence of unmelt particles is attributable to the incomplete melting of 8YSZ powders. With a high melting point and a low thermal conductivity, 8YSZ powders are unlikely to melt thoroughly in the heating, deformation and cooling processes of plasma spraying. The unmelt particles led to a rough and uneven surface structure.

Figure 9 (b) is the surface morphology of the laser-remelted coating. It can be seen that the coating surface was relatively smooth, and the unmelt particles disappeared. This is because
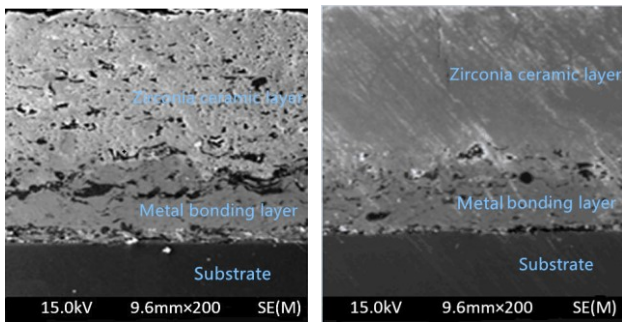
the unmelt ceramic powders were sufficiently melted thanks to the rapid rise in coating surface temperature during laser remelting. When the laser beam moved away, the powders solidified and recrystallized quickly, resulting in fine grains, a uniform microstructure and a smooth surface.
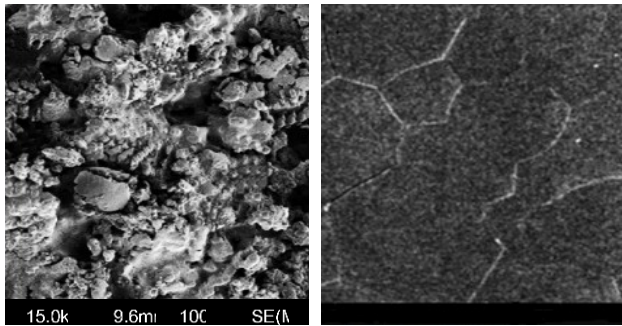
(a) Plasma-sprayed coating (b) Laser-remelted coating

Figure 9. Coating surface morphology

Figures 10 (a) and (b) shows the fractured cross-section morphology of plasma-sprayed 8YSZ coating and laser-remelted coating, respectively. From bottom to top, the cross-section consists of the substrate, the metal bonding layer, and the ceramic top layer.

(a) Plasma-sprayed coating (b) Laser-remelted coatin

Figure 10. Fractured cross-section morphology

As shown in Figure 10 (a), clear boundaries were observed between different layers, and the layers were combined loosely via physical and mechanical bonds. The cross-section of plasma-sprayed coating contained lots of pores and cracks. It can be seen from Figure 10 (b) that the number of pores and cracks reduced dramatically after laser remelting, and the inter-layer boundaries were blurred. The microstructure comparison of the two coatings shows that the coating quality was remarkably improved through laser remelting.

4.3 Thermal shock test

The roller works under a periodic but varying temperature stress, due to the cyclic action of heat transfer from the high-temperature slab and the water cooling effect. Under thermal shock, the thermal stress will increase because the ceramic top layer and matrix material differ in thermal expansion coefficient. When the thermal stress reaches a certain threshold, cracks will appear, and even cause coating failure [17]. Therefore, it is necessary to study the thermal shock resistance of the coating.

Several thermal shock tests were conducted by heating and quenching. The Φ20*30 cylindrical specimens were heated at

1,000°C for 10min in a box type heating furnace, and then thrown into cool water. During the tests, the cool water temperature was maintained at 20~25°C. When the samples were cooled down to the room temperature, they were taken out, dried and put into the furnace again. This process was repeated until nearly 10% of the coating surface peeled off. The number of thermal cycles after the thermal shock failure was defined as the thermal cycling lifetime of the specimen.

Figure 11 shows the macroscopic morphology of plasma-sprayed coatings after thermal shock tests. Macroscopic cracks appeared at the end of the cylindrical sample after 14 thermal cycles. With the increase in the number of cycles, the quenching-induced heat was released from the cracks, leading to a high thermal stress. Under the joint action of thermal oxide layer and thermal stress, the coating peeled off across a large area. The exfoliation continued to worsen until the coating failed at the 32nd thermal cycle.
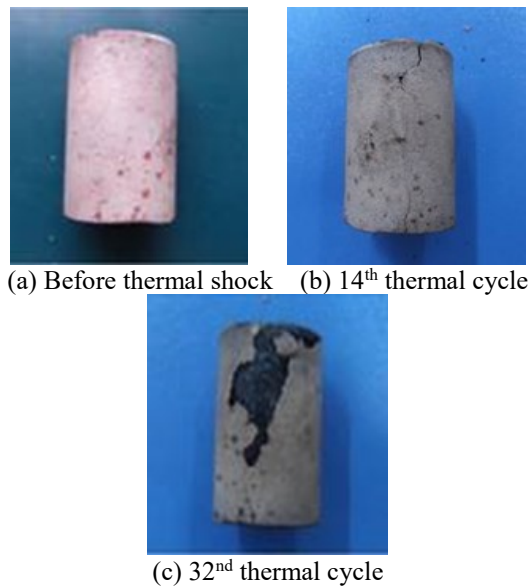

(a) Before thermal shock   (b) 14th thermal cycle

(c) 32nd thermal cycle

Figure 11. Post-thermal shock morphology of plasma-sprayed samples

(a) Before thermal shock   (b) 43rd thermal cycle

(c) 94th thermal cycle

Figure 12. Morphology of laser-remelted samples after thermal shock

Figure 12 shows the macroscopic morphology of laser-remelted coatings after thermal shock tests. Unlike the plasma-spraying coatings, the laser-remelted coatings suffered from no obvious macroscopic cracks during the tests. The thermal shock failure of laser-remelted TBCs was dominated by local exfoliation. After 43 thermal cycles, small pieces of the coating started to flake away from the top of the cylindrical sample. With the increase in the number of thermal cycles, more and more places underwent exfoliation, creating an ever-increasing area of spalling. The top ceramic coating peeled off in large areas at the 94th thermal cycle. Compared with plasma-sprayed coatings, the laser-remetled coatings had a much greater resistance to thermal shock.

The coating damages are mainly caused by the following factors: the thermal stress produced in the TBC under thermal shock, the thermally grown oxide (TGO) generated at the interface between the top ceramic layer and the bond layer, and the phase transformation stress [19, 20]. The plasma-sprayed coatings had a laminated structure with many horizontal cracks, especially at the interface, while the laser-remelted coatings had a columnar structure in the ceramic layer. The columnar structure boasts a better resistance to thermal shock in thermal cycles than the laminated structure. In addition, the vertical cracks in the remelted coating can release part of the stress accumulated in thermal cycles, which further improves the thermal shock resistance of the coatings [21].

5. PERFORMANCE ANALYSIS OF CONVENTIONAL COATINGS AND NANOSCALE COATINGS

5.1 Surface morphology comparison

The effect of zirconia with different specifications on coating properties were analysed and discussed to obtain better TBCs. The morphologies of as-prepared nanoscale and conventional zirconia powders were observed with were observed with an S-4800 field emission SEM (Hitachi).

Figures 13(a) and 13(b) display the SEM images of the conventional zirconia powder and the nanometre zirconia powder, respectively. It is clear that the conventional powder was polyhedral and irregular in shape, while the nanometre powder was nearly spherical or ellipsoidal. The morphology of nanometre powder is featured by good flowability and high density, making the powder suitable for plasma spraying.

The two types of zirconia powders were adopted to prepare remelted coatings (hereinafter referred to as the conventional coating and the nanoscale coating). The surface morphologies of the two coatings were observed by an OLS 3100 confocal laser scanning microscope. As can be seen from Figures 14(a) and 14(b), both of the two coatings had retiform micro-cracks and corrugated bulges after laser remelting. The surface morphologies are resulted from the low fracture toughness of the ceramic material [22]. The material was easily cracked in the heating and cooling cycles during the laser remelting process. In addition, the high viscosity of the melting ceramic during the heating process also contribute to the crack formation. The viscous melting ceramic trapped the gases produced by expansion, adding to the possibility of cracking. Comparatively speaking, the coating prepared from nanoscale powders had much less reticulated cracked than the conventional coating. This may be related to the high toughness of nanoscale zirconia coatings.
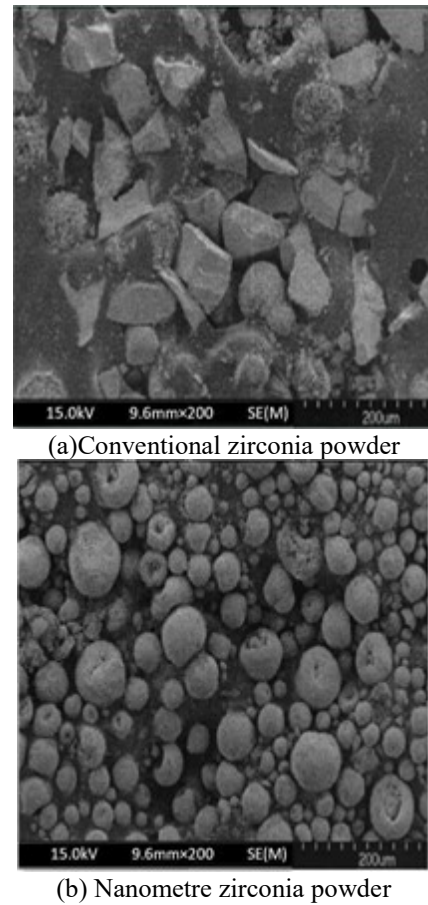

(a)Conventional zirconia powder

(b) Nanometre zirconia powder

Figure 13. SEM images of zirconia powders

(a) Conventional coating morphology
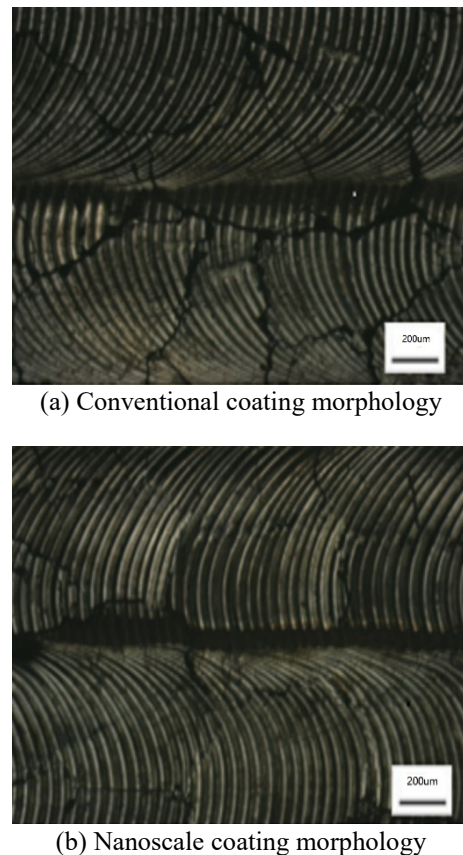

(b) Nanoscale coating morphology

Figure 14. Surface morphology of remelted coatings

5.2 Thermal shock test

By the same method as before, a thermal shock test was conducted on the two types of coatings. Figure 15 show the macroscopic diagrams of the conventional and nanoscale coating samples at the 60th, 90th, and 150th thermal cycles. The thermal shock test results are summed up in Table 5. After 60 thermal cycles, neither the conventional nor the nanoscale TBCs produced microcracks or exfoliation. After 90 thermal cycles, both types of coatings suffered from different degrees of exfoliation, microcracking and bulging. For the nanoscale coating, only about 5% of it experienced exfoliation, much smaller than that (18%) of the conventional coating.

Table 5. Thermal shock test results on two types of remelted coatings

Coating specification	Thermal cycle 60 times	Thermal cycle 90 times	Thermal cycle 150 times
Conventional level off ratio	0	18%	60%
Nanostructured off ratio	0	5%	20%
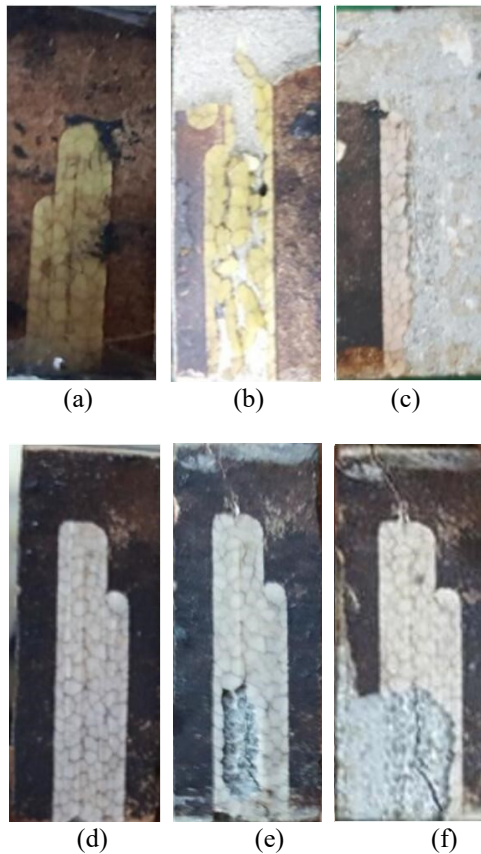
(a) Conventional coating at 60th thermal cycle
(b) Conventional coating at 90th thermal cycle
(c) Conventional coating at 150th thermal cycle
(d) Nanoscale coating at 60th thermal cycle
(e) Nanoscale coating at 90th thermal cycle
(f) Nanoscale coating at 150th thermal cycle

Figure 15. Macroscopic diagrams of conventional and nanoscale coatings

After 150 thermal cycles, the conventional coating was mostly fallen off with no cracks on the matrix, while about 20% of the nanoscale coating fell off with a noticeable crack on the matrix. Both specimens suffered from serious deformations. The failure of the conventional sample was initiated by the spalling of the ceramic coating, while the failure of the nanoscale sample was induced by the high inner heat stress from the mismatch of thermal expansion coefficient between ceramic top and metal matrix. Under the breaking tension produced by the matrix crack, the ceramic layer was stretched all the way towards TBC cracking.

Through the comparison, it is clear that the nanoscale coating outperformed the conventional one in thermal shock resistance. The edge in performance is related to the coating toughness and porosity. With a relatively high toughness and low porosity, the nanoscale coating inhibits the crack propagation, and has only a few microcracks. Hence, the nanoscale zirconia powders can greatly enhance the thermal shock resistance of coatings.

6. CONCLUSIONS

The FEM analysis shows that the 8YSZ coating can reduce the surface temperature of the pulling-straightening roller. The reduction of surface temperature inevitably suppresses the thermal stress, which in turn lowers the effect of thermal shock on the roller surface. It is proved that the TBCs can extend the service life of the roller.

In contrast to conventional plasma-sprayed coating, both laser remelting and nanoscale zirconia particles can reduce the number of pores and microcracks in the coatings, and thus enhance the quality of the TBCs. The two methods also contribute to the thermal shock resistance of the TBCs. This research on TBC properties lays a solid basis for the application of the TBC on pulling-straightening roller.

REFERENCES

[1] Li J., Sun D.Y., Zhang F. (2017). Properties of nano ZrO$_2$ coating on roller surface of continuous casting machine, *Iron & Steel*, Vol. 52, No. 10, pp. 104-108. DOI: 10.13228/j.boyuan.issn0449-749x.20170114

[2] Turki A.E., Allen G.C., Younes C.M. (2015). An investigation of the effect of thermal cycling on plasma-sprayed zirconia/NiCoCrAlY thermal barrier coating, *Materials & Corrosion*, Vol. 55, No. 1, pp. 24-29. DIO: 10.1002/maco.200303709

[3] Xu S.M, Zhang J.M., Dong Y.J. (2015). Application of zirconia thermal barrier coating in roller of liquid core heavy reduction mill, *Journal of Plasticity Engineering*, Vol. 22, No. 2, pp. 132-137. DOI: 10.3969/j.issn.1007-2012.2015.02.024

[4] Gok M.G., Goller G. (2015). Microstructural evaluation of laser remelted gadolinium zirconate thermal barrier coatings, *Surface & Coatings Technology*, No. 276, pp.

202-209. DOI: 10.1016/j.surfcoat.2015.06.074

[5] Munez C.J., Gomez G.J., Sevillano F. (2011). Improving thermal barrier coatings by laser remelting, *Journal of Nanoscience &Nanotechnology*, Vol. 11, No. 10, pp. 8724-8729. DOI: 10.1166/jnn.2011.3457

[6] Liu W.M., Sheng T.Y., Kong D.J. (2017). Effects of laser remelting on surface interface morphologies, bonding modes and corrosion performances of arcsprayed Al coating, *Anti-Corrosion Methods and Materials*, Vol. 64, No. 1, pp. 43-51. DOI: 10.1108/ACMM-11-2015-1591

[7] Fan Z.J., Wang K.D., Dong X. (2016). The role of the surface morphology and segmented cracks on the damage forms of laser re-melted thermal barrier coatings in presence of a molten salt (Na_2SO_4+V_2O_5), *Corrosion Science*, Vol. 11, No. 1, pp. 56-67. DOI: 10.1016/j.corsci.2016.11.011

[8] Hao Y.F., Tian Z.J., Liu T. (2010). Microstructure and properties of plasma sprayed nanostructured thermal barrier coatings before and after laser glazing, *Aerospace Materials & Technology*, No. 2, pp. 88-90.

[9] Li Q.L. (2014). Research on the failure of plasma sprayed ZrO_2 coatings thermal shock, *China Surface Engineering*, Vol. 17, No. 3, pp. 17-25.

[10] Sun D.Y., Hou G.Y., Zhang J.Y. (2014). Improving rolls thermal shock resistance by roller by cladding $ZrO_2$8%Y_2O_3 coating, *Journal of Yanshan University*, Vol. 38, No. 3, pp. 216-220.

[11] Li J.F., Watanabe R. (2010). Phase transformation in Y_2O_3-partially-stabilized ZrO_2 polycrystals of various grain sizes during low-temperature aging in water, *Journal of the American Ceramic Society*, Vol. 81, No. 10, pp. 2687-2691. DOI: 10.1016/j.surfcoat.2015.06.074.

[12] Sun D.Y., Zhang Y.F., Zha X.W. (2011). Thermal mechanical coupling analysis and fatigue life calculation of rolling mill roll with liquid core, *Journal of Yanshan University*, Vol. 35, No. 1, pp. 40-45.

[13] Ye D.L., Hu J.H. (2002). *Practical Handbook of Thermo-Dynamic Data of Inorganic Materials*, Metallurgical Industry Press, Beijing, pp. 77-79.

[14] Alam M.S., Islam T., Rahman M.M. (2015). Unsteady hydromagnetic forced convective heat transfer flow of a micropolar fluid along a porous wedge with convective surface boundary condition, *International Journal of Heat and Technology,* Vol. 33, No. 2, pp. 115-122. DOI: 10.18280/ijht.330219.

[15] Zhan N.Y., Xu Y., Wang Z.Y. (2015). Research on heat-transfer and three-dimensional characteristics of natural convection in a small cavity with heat sources, *International Journal of Heat and Technology*, Vol. 33, No. 3, pp. 59-66. DOI: 10.18280/ijht.330308.

[16] Duan X., Li D.Y. (2009). The thermal-structural coupling analysis and fatigue life's prediction research of roll shell in continuous roll casting, *Mechanical Design and Manufacture*, No. 1, pp. 137-138.

[17] Yu Q.H., Rauf A, Wang N. (2011). Thermal properties of plasma-sprayed thermal barrier coating with bimodal structure, *Ceramics International*, Vol. 37, No. 3, pp. 1093-1099. DOI: 10.1016/j.ceramint.2010.11.033

[18] Liu Z.G., Zhang W.H., Ouyang J.H. (2014). Novel double-ceramic-layer $(La_{0.8}Eu_{0.2})_2Zr_2O_7$/YSZ thermal barrier coatings deposited by plasma spraying, *Ceramics International*, No. 40, pp. 11277-11282. DOI: 10.1016/j.ceramint.2014.03.159

[19] Chen W.R., Wu X, Marple B.R. (2006). The growth and influence of thermally grown oxide in a thermal barrier coating, *Surface & Coating Technology*, Vol. 201, No. 3, pp. 1074-1079. DOI: 10.1016/j.surfcoat.2006.01.023

[20] Tang F., Ajdeisztajn L, Kim G.E. (2006). Effects of variations in coating materials and process conditions on the thermal cycle properties of NiCrAlY/YSZ thermal barrier coatings, *Materials Science & Engineering,* Vol. 425, No. 1, pp. 94-106. DOI: 10.1016/j.msea.2006.03.043

[21] Duan Z.Y., Wang D.S. (2012). Improving Thermal Shock Resistance of Plasma-sprayed Yttria-stabilized zirconia thermal barrier coatings by laser remelting, *Advanced Materials Research*, No. 472, pp. 2502-2507. DOI: 10.4028/www.scientific.net/AMR.472-475.2502

[22] Han M., Huang J.H, Chen S.H. (2013). Research progress and review on key problems of stress and failure mechanism of thermal barrier coating, *Journal of Aeronautical Materials*, Vol. 33, No. 5, pp. 83-98. DOI: 10.3969/j.issn.1005-5053.2013.5.014